J|A|C|S COMMUNICATIONS

Published on Web 11/07/2006

Preparation of Hierarchically Porous Nickel from Macroporous Silicon

Xi Zhang and King-Ning Tu*

Department of Materials Science and Engineering, University of California at Los Angeles, Los Angeles, California 90095

Received April 12, 2006; E-mail: kntu@ucla.edu

Porous metals are known to be useful in many fields such as catalysis, batteries, fuel cells, capacitors, sensors, and so on.[1−6] In particular, free-standing metal films with hierarchical porous architectures possess significant advantage for many chemical applications. For instance, such a feature is practically helpful to microfluidic-based sensors in that bimodal pore size distribution composed of large porosity channels and highly porous channel walls is desirable in order to achieve both fast response time and high sensitivity. In this work, we are disclosing a novel strategy of preparing nickel hierarchical porous structure with cylindrical microchannels and nanoporous sidewalls.

Today, template-directed methods have been largely adopted to fabricate porous materials (ceramics, polymers, semiconductors, etc.) with unimodal pore size distribution. Both mesoporous (pore $<$50 nm) and macroporous ($>$50 nm) metals with controlled pore size have been reported by people in the past decade. Typically, porous metals with cylindrical voids were replicated via templates of either liquid-crystalline surfactant assemblies or anodically etched alumina membranes.[7,8] Recently, macroporous metals with larger scale pore size have been fabricated by using colloidal fcc crystals.[9,10] Thus ordered and interconnected spherical voids were generated in metals.[11] Despite a precise control over the final size and structure of porous metals, these techniques, however, required further steps to remove the initial nonmetallic skeleton. We have been studying a one-step replicative method which is less difficult and time-consuming. Porous nickel was fabricated as a direct positive replica of the template.

Macroporous silicon was selected as the template. On the smooth surface of low doped p-type (100) silicon, straight microchannels were formed by anodization in a two-electrode Teflon cell containing the HF solution.[12] Macropore formation in silicon has been extensively investigated since the 1990s. The morphology is determined by parameters such as resistivity, current density, HF concentration, nature of solvent, etching time, etc. Accordingly, pore diameter can range from submicron to a few micrometers under special control. The aspect ratio of the etched channels can be more than 200 with extended hours' treatment.

We have employed a wet templating process through which nickel was deposited at the expense of silicon. Deposition was electrolessly carried out in an alkaline aqueous nickel bath at a temperature of 60 °C. Not like a conventional electroless nickel solution, the commonly contained reducing agent (e.g., sodium hypophosphite) was excluded. On the other hand, an amount of 2.5 M ammonium fluoride was added in the solution to work with silicon and the solution interface. The solution contained another 1.0 M nickel sulfate as the metal ion source and was buffered by 0.5 M ammonium sulfate. The overall pH was adjusted to 8 by ammonia. After immersion of the macroporous silicon in our nickel bath, displacement reactions did occur between the nickel ions in the solution and the silicon atoms on the macropore sidewalls due to the difference of individual equilibrium redox potentials between nickel and silicon in the system. That is to say, nickel was reduced

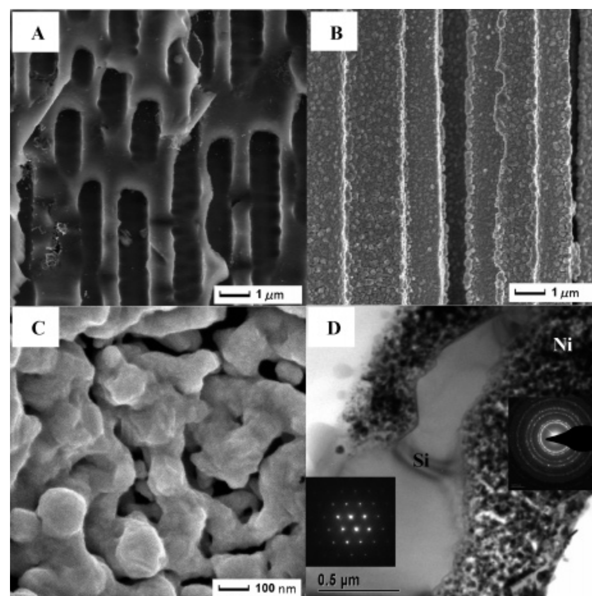

Figure 1. (A) Cross-sectional SEM image of the Si macroporous structure. (B) Cross-sectional SEM image after Ni replication of the Si template. (C) High-magnification SEM image of the Ni-replicated sidewall morphology. (D) TEM image of the half-replicated sidewall cross-section with Si and Ni deposits (Si and Ni diffraction patterns inset). All SEM images were acquired on a JEOL JSM-6700. TEM images were acquired on a FEI/Philips CM-200.

and deposited via electron exchange with silicon that was concurrently oxidized and dissolved in the fluoride-containing media.[13] Having been studied earlier, ammonium fluoride kept the nickel solution in an alkaline state and gave rise to a state of highly corrosive activity on silicon surface so that the kinetics of overall displacement reactions was accordingly enhanced.[14] Commonly used in buffered oxide etching (BOE), ammonium fluoride is very toxic and must be operated with extreme caution.

The first significant observation from the process was the non-self-limiting nickel replacement behavior resulting in a complete material change from silicon to nickel on the channel sidewalls after wet treatment for hours. The original framework was well maintained. What should be highlighted here is that no further steps were needed with regard to removing the template skeleton, but all occurred in a simple immersion step. Chemical composition of the sample before and after immersion was evaluated by energy dispersive X-ray analysis (EDX) during scanning electron micro-imaging of the cross-sections, confirming whole conversion from silicon to nickel. SEM micrographs in Figure 1 show the positive metal replica (Figure 1b), as compared to the silicon template prior to the wet treatment (Figure 1a). Straight channels on the scale of 1 μm can be seen in both the original silicon and the resultant nickel structures.

It is commonly thought that the displacement deposition would be terminated once the silicon sidewall surface was fully covered

10.1021/ja062562+ CCC: $33.50 © 2006 American Chemical Society

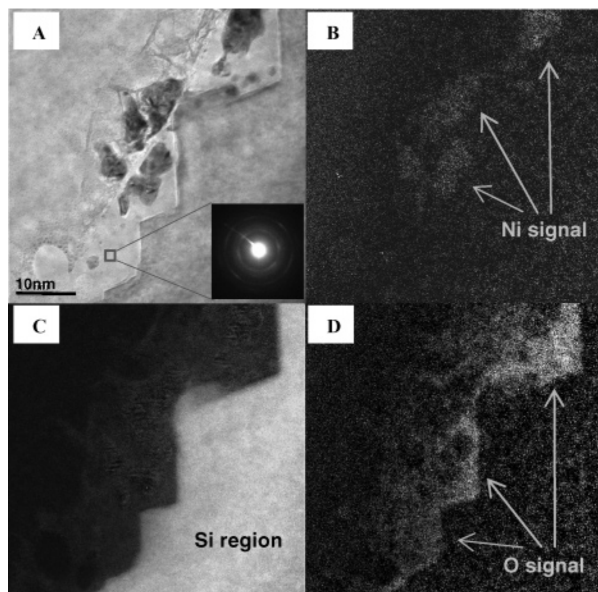

Figure 2. (A) EELS image of sidewall cross-section with displacement reactions on the surface. Ni deposits and Si skeleton are visible along with an intermediate material recognized to be silicon oxide. Its electron diffraction pattern is inserted on the right bottom corner. (B) EELS Ni-L map. (C) EELS Si-K map. (D) EELS O-K map.

by nickel deposits. However, observation of such total replacement remained questionable. After taking a finer characterization over the sidewall morphology, we acquired the image (Figure 1c) that can help improve the understanding of why nickel was replicating silicon on the sidewalls during the process and a metallic structure was consequently generated. Apparently, the formed nickel deposits consist of delicate nanoscale features that are superimposed over the overall macroporous structure. The discernible nanoporosity on the sidewalls now is considered to be a straight outcome of the deposition process and not to exist on the original skeleton. What would make sense is that such an existence of these voids when interconnected could assist the diffusion of the aqueous solution through as-deposited nickel to further replicate the sidewall. The ultimate structure is a nickel film with micron-sized channels and nanoporous channel sidewalls. Transmission electron micrograph (Figure 1d) shows the cross-section of one sidewall in the midst of the nickel replication. Silicon and nickel were both identified by electron diffractions (see the inset patterns). As can be seen from the silicon diffraction, silicon pores were initially etched in the <100> direction. Upon nickel replication of porous silicon, BET surface area was increased by about 6.19 m^2/g from its original 5.16 m^2/g. This increase was ascribed to the as-formed accessible nanopores of average size around 54.38 Å by BET calculation.

In order to explain the generation of nanoporosity on sidewalls during the nickel deposition, we conducted electron energy loss spectroscopic (EELS) analysis in TEM. Micrographs in Figure 2 have captured a cross-sectional area covering the displacement reaction interface. EELS mappings were made, respectively, for nickel, silicon, and oxygen. In the zero-energy loss image (Figure 2a), nickel deposits were seen clustered. Nickel mapping at the L edge is displayed in Figure 2b. Silicon mapping at the K edge can be viewed in Figure 2c. A type of intermediate material (brightly contrasted in Figure 2a) that separates nonreacted silicon and nickel deposits on the sidewalls is of interest. Judging from silicon and oxygen mapping at the K edge (Figure 2d) together, we could see the existence of both silicon and oxygen. Therefore, oxide formation was highly probable midway in the reactions and could be a result of silicon anodization that is one of the redox couples. This shall be in agreement with the displacement principle that nickel is reduced by oxidizing silicon. Using a convergent e-beam, EDX confirmed the ratio of silicon to oxygen was roughly 1 over a sensitive dimension of 20 nm. The diffuse diffraction pattern (Figure 2a, inset) exhibited amorphous nature of the intermediate. It would be recognized as silicon sub-oxide. In a previous study on nickel displacement deposition on a blanket silicon surface in an aqueous alkaline solution, it was found that the deposition reaction was initiated by the formation of sub-oxide at the interface, and sub-oxide species can serve as “reductant” for nickel ions.[15] In other words, silicon sub-oxide formed as an intermediate phase could experience successive oxidation steps and contribute to nickel deposition up until full Si oxidation. Now in our fluoride medium, oxides would be eventually etched and dissolved, in a way, by F^-.

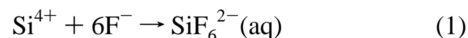

$$Si^{4+} + 6F^- \rightarrow SiF_6^{2-}(aq) \quad (1)$$

So it is reasonable to expect a nonpassivated state for current displacement reactions to occur continuously, resulting in highly porous nickel sidewalls eventually due to removal of the silicon dioxide. Silicon dioxide had been observed together with nickel deposits when using a solution containing no ammonium fluoride and finally inhibited the deposition reactions due to its insulating property.[15] With fluoride added, the oxide was etched away to make the deposits porous and reactions nonterminated. In addition, formation of silicon(111) microfacets was previously reported during silicon etching in ammonium fluoride.[16] Such an anisotropic anodizing behavior along a specific direction can be seen in Figure 2a as well in our solution containing fluoride. With its existence, the (111) microfacets were generated soon after the immersion.[17]

In summary, this work demonstrates a technique of preparing hierarchical porous nickel architectures through an easy, one-step templating process. Our strategy is able to create metallic nickel structure with bimodal pore size distribution. Such methodology could be generic for production of other metals if they possess the same redox relation to silicon in the mixed system, namely, higher original equilibrium redox potentials than that of silicon. Good examples are the noble metals which are being investigated.

Acknowledgment. The authors thank Mr. Chih-Hang Tung for assistance with TEM characterization and discussion. This research is supported by both the Semiconductor Research Corporation under Contract No. 2001-NJ-936 and the National Science Foundation under Contract No. ECS-0120368.

References

(1) Leroux, F.; Koene, B. E.; Nazar, L. F. *J. Electrochem. Soc.* **1996**, *143*, L181.
(2) He, X.; Antonelli, D. *Angew. Chem., Int. Ed.* **2001**, *41*, 214.
(3) Ye, S.; Vijh, A. K.; Dao, L. H. *J. Electrochem. Soc.* **1996**, *143*, L7.
(4) Pell, W. G.; Conway, B. E. *J. Power Sources* **1996**, *63*, 255.
(5) Wang, J.; Agnes, L. *Anal. Chem.* **1992**, *64*, 456.
(6) Tierney, M. J.; Kim, H. L. *Anal. Chem.* **1993**, *65*, 3435.
(7) Attard, G. S.; Bartlett, P. N.; Coleman, N. R. B.; Elliott, J. M.; Owen, J. R.; Wang, J. H. *Science* **1997**, *278*, 838.
(8) Masuda, H.; Fukuda, K. *Science* **1995**, *268*, 1466.
(9) Velev, O. D.; Tessier, P. M.; Lenhoff, A. M.; Kaler, E. W. *Nature* **1999**, *401*, 548.
(10) Jiang, P.; Bertone, J. F.; Colvin, V. L. *Science* **2001**, *291*, 453.
(11) Jiang, P.; Cizeron, J.; Bertone, J. F.; Colvin, V. L. *J. Am. Chem. Soc.* **1999**, *121*, 7957.
(12) Lehmann, V. *J. Electrochem. Soc.* **1993**, *140*, 2836.
(13) Gorostiza, P.; Kulandainathan, M. A.; Díaz, R.; Sanz, F.; Allongue, P.; Morantec, J. R. *J. Electrochem. Soc.* **2000**, *147*, 1026.
(14) Chela, M.; Homma, T.; Bertagna, V.; Erre, R.; Kubo, N.; Osaka, T. *J. Electroanal. Chem.* **2003**, *559*, 111.
(15) Niwa, D.; Homma, T.; Osaka, T. *J. Phys. Chem. B* **2004**, *108*, 9900.
(16) Niwano, M.; Kondo, Y.; Kimura, Y. *J. Electrochem. Soc.* **2000**, *147*, 1555.
(17) Yau, S. L.; Kaji, K. *Appl. Phys. Lett.* **1995**, *66*, 766.

JA062562+